CHEMISTRY
A EUROPEAN JOURNAL

DOI: 10.1002/chem.201003573

4,4′-Dithiobisdipicolinic Acid: A Small and Convenient Lanthanide Binding Tag for Protein NMR Spectroscopy

Xinying Jia,[a] Ansis Maleckis,[a, b] Thomas Huber,[a] and Gottfried Otting*[a]

Abstract: Pseudocontact shifts (PCS) from paramagnetic lanthanide ions present powerful long-range structure restraints for studies of proteins by nuclear magnetic resonance spectroscopy. To elicit PCSs, the lanthanide must be attached site-specifically to the target protein. In addition, it needs to be attached rigidly to avoid averaging of the PCSs due to mobility with respect to the protein and it must not interfere with the function of the protein. Here, we present a dipicolinic acid reagent that spontaneously forms a disulfide bond with thiol groups of accessible cysteine residues. A minimal number of rotatable bonds between the cysteine side chain and the tag helps to minimise mobility. Combined with the small size of the tag and quantitative tagging yields, these features make it a highly attractive tool for generating structure restraints by paramagnetic lanthanides.

Keywords: lanthanides · NMR spectroscopy · protein labeling · pseudocontact shifts · thiol-reactive reagent

Introduction

Paramagnetic lanthanide ions produce pronounced effects in protein NMR spectra. Among the paramagnetic effects, pseudocontact shifts (PCSs) are most easily measured as the difference in chemical shifts between NMR spectra recorded in the presence of paramagnetic and diamagnetic metal ions. As PCSs can be observed over distances greater than 40 Å from the metal ion,[1] they present outstandingly useful long-range distance restraints.

The PCS $\Delta\delta^{PCS}$ (in ppm) of a nuclear spin depends on its polar coordinates r, θ and ϕ with respect to the principal axes of the magnetic susceptibility anisotropy tensor ($\Delta\chi$ tensor):[2]

$$\Delta\delta^{PCS} = \frac{1}{12\pi r^3}\left[\Delta\chi_{ax}\left(3\cos^2\theta - 1\right) + \frac{3}{2}\Delta\chi_{rh}\sin^2\theta\cos 2\varphi\right] \qquad (1)$$

where $\Delta\chi_{ax}$ and $\Delta\chi_{rh}$ denote, respectively, the axial and rhombic components of the $\Delta\chi$ tensor, which describes the anisotropy of the magnetic susceptibility of the paramagnetic centre. In effect, the principal axes of the $\Delta\chi$ tensor present a coordinate frame that is anchored to the protein structure and centred on the metal ion. Owing to their long-range nature, lanthanide-induced PCSs contain powerful information for NMR resonance assignments, studies of domain mobility[3,4] and structure determinations of proteins[5] and protein–protein[6,7] and protein–ligand complexes (for a recent review see ref. [8]).

To generate PCSs, however, the lanthanide must be site-specifically and rigidly attached to the target protein. As most proteins are devoid of natural lanthanide binding sites, this has spurred the development of a wide range of methods to attach lanthanides to proteins, including peptide tags that can be fused to the N or C terminus of proteins, tags that can be attached through disulfide bonds and tags that associate with proteins in a non-covalent fashion (for reviews see refs. [9], [10]). The most popular approach uses thiol groups of cysteine residues for chemical modification with a lanthanide binding tag by one or two disulfide bonds.[7,11–19] Best immobilisation of the lanthanide ion is accomplished by tags that are associated with the protein at two attachment sites, either via two disulfide bonds[13,15,16] or through an N-terminal fusion and a disulfide bond.[7,19]

Dipicolinic acid (DPA) tags stand out for their small size and rigid lanthanide coordination.[18,20] DPA binds lanthanides with nanomolar dissociation constant although it is only a tridentate ligand.[21] In contrast to ethylenediaminetetraacetic acid (EDTA) derivatives, DPA binds lanthanides in a non-chiral fashion, so that no diastereomers are produced when lanthanides bind to protein–DPA adducts[12,22] In addition, the free coordination sites of the lanthanide are thus readily available for additional interactions with carboxyl groups of acidic amino acid side chains of the protein, which helps to immobilise the lanthanide ion.[18] The smallest lanthanide binding tag produced to date is 3-mercapto-2,6-pyridinedicarboxylic acid (3MDPA; Scheme 1D).[20] The more symmetrical 4-mercapto-DPA analogue (4MDPA; Scheme 1A) is equally small and features the same small

[a] Dr. X. Jia,[+] A. Maleckis,[+] Dr. T. Huber, Prof. G. Otting
Research School of Chemistry
Australian National University, Canberra, ACT 0200 (Australia)
Fax: (+61) 2-61250750
E-mail: gottfried.otting@anu.edu.au

[b] A. Maleckis[+]
Latvian Institute of Organic Synthesis, Riga, 1006 (Latvia)

[+] These authors contributed equally to the work.

Supporting information for this article is available on the WWW under http://dx.doi.org/10.1002/chem.201003573.

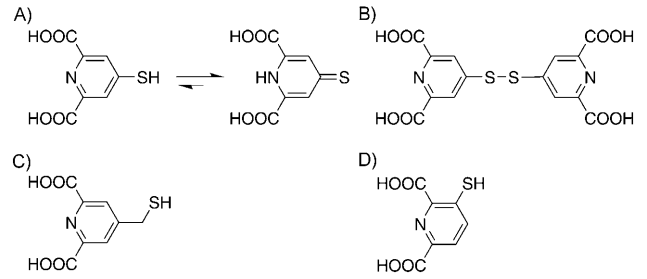

Scheme 1. Tautomeric equilibrium of 4MDPA and structures of different DPA tags. a) Tautomeric equilibrium of 4MDPA. b)–d) Structures of the 4MDPA dimer (4,4′-disulfanediyldipyridine-2,6-dicarboxylic acid), 4MMDPA (4-methylmercapto-dipicolinic acid) and 3MDPA, respectively.

number of rotatable bonds. Preliminary experiments, however, showed that the thiol group is unreactive in aqueous solution due to a tautomeric equilibrium that is shifted towards the thioketo form (Scheme 1 a[40]).

Here we show that, because the thioketo form of 4MDPA is a good leaving group, the oxidised form of 4MDPA (Scheme 1B) can be used as a thiol-reactive reagent that spontaneously adds a 4MDPA moiety to cysteine thiol groups in aqueous solution at neutral pH. This makes the reagent very convenient to use and produces high yields of tagged protein. In addition, the symmetry of the tag minimises the possibility of alternative conformations that could reduce the size of PCSs by conformational exchange.

Results

Synthesis of the 4MDPA dimer: The synthesis of the 4MDPA dimer is depicted in Scheme 2. The synthesis started from commercially available chelidamic acid (**1**). Following protection of the carboxyl groups as *tert*-butyl esters, the carbonyl oxygen of the chelidamic acid was substituted by sulphur by using Lawesson′s reagent to obtain **2**. Oxidation of **2** with H_2O_2 in acetonitrile afforded the desired disulfide in only about 70% purity. The corresponding sulfide (tetra-*tert*-butyl-4,4′-sulfanediyldipyridine-2,6-dicarboxylate) was formed as the main side product and was difficult to separate by column chromatography. Better purity (about 90%), however, was achieved by using H_2O_2 in biphasic CH_2Cl_2/H_2O with Bu_4NCl as phase-transfer catalyst. Removal of the *tert*-butyl groups in CH_2Cl_2/TFA yielded product **4**. The final product still contained about 10% of the sulfide analogue. As the sulfide analogue does not interfere with the ligation of proteins, the product was used without further purification. It has been made commercially available by ASLA Biotech (Latvia).

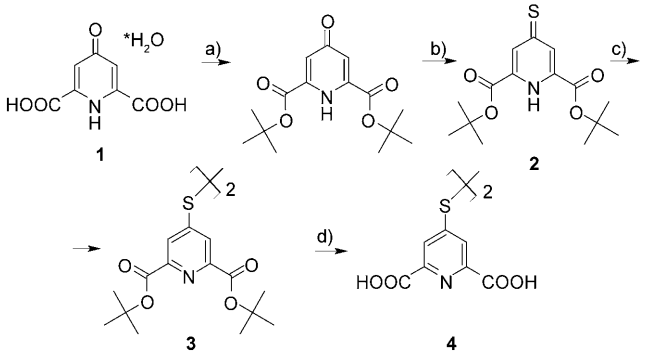

Scheme 2. Synthesis of dimeric 4,4′-dithiobis-dipicolinic acid (**4**): a) isobutylene, $HClO_4$, CH_2Cl_2; b) Lawesson′s reagent, toluene; c) H_2O_2, Bu_4NCl, CH_2Cl_2/H_2O; d) trifluoroacetic acid (TFA), CH_2Cl_2.

Tagging of proteins with 4MDPA: Experiments were performed with uniformly ^{15}N-labelled samples of the N-terminal DNA-binding domain of the *Escherichia coli* (*E. coli*) arginine repressor (ArgN)[23] and the C379S mutant of the intracellular domain (ICD) of the rat p75 neurotrophin receptor (p75ICD).[24] ArgN and p75ICD contained a single cysteine residue at position 68 and 416, respectively. The proteins were ligated with 4MDPA by adding solutions of the proteins ($\approx$0.5 mM) to a solution of the 4MDPA dimer (5 mM), producing the adducts ArgN–4MDPA and p75ICD–4MDPA, respectively. The ligated protein products were purified by chromatography by using either SP sepharose (ArgN–4MDPA) or DEAE sepharose columns (p75ICD–4MDPA).

NMR resonance assignments of the protein–4MDPA adducts: As observed previously for ArgN–3MDPA[20] and ArgN–4MMPDA,[18] ^{15}N HSQC cross-peaks of residues near Cys68 were broadened, indicating conformational exchange on the millisecond time scale. In contrast, the ^{15}N HSQC spectrum of p75ICD–4MPDA did not show any evidence of exchange broadening and only minor changes in chemical shifts between ligated and unligated protein, as expected for a highly solvent-exposed cysteine residue[25] In the course of titrating the samples with Y^{3+}, cross-peaks of the complex appeared, whereas those of the apo forms decreased, indicating that the exchange of metal ion was slow on the NMR time scale (milliseconds). The solutions remained clear throughout the experiments. The resonance assignments of the ^{15}N HSQC spectra of the diamagnetic Y^{3+} complexes were verified by 3D NOESY–^{15}N HSQC spectra. Conserved NOE patterns indicated structural conservation. Chemical-shift changes were limited to amides in the vicinity of the tagged cysteine residues.

PCS measurements: Significant PCSs were observed in the 1:1 complexes of ArgN and 4MDPA with Ce^{3+}, Tb^{3+}, Tm^{3+} and Yb^{3+}, by using the complex with Y^{3+} as the diamagnetic reference (Figure 1). PCSs were also observed with Co^{2+} by using Zn^{2+} as the diamagnetic reference (Figure S1 in the Supporting Information). Exchange broadening observed in the absence of metal ions vanished upon formation of the ArgN–4MDPA–metal complexes.

To assess the lanthanide binding affinity of the ArgN–4MDPA adduct, we titrated ArgN–4MDPA with a 1:1 complex of Yb^{3+} and DPA. The resulting ^{15}N HSQC spectrum

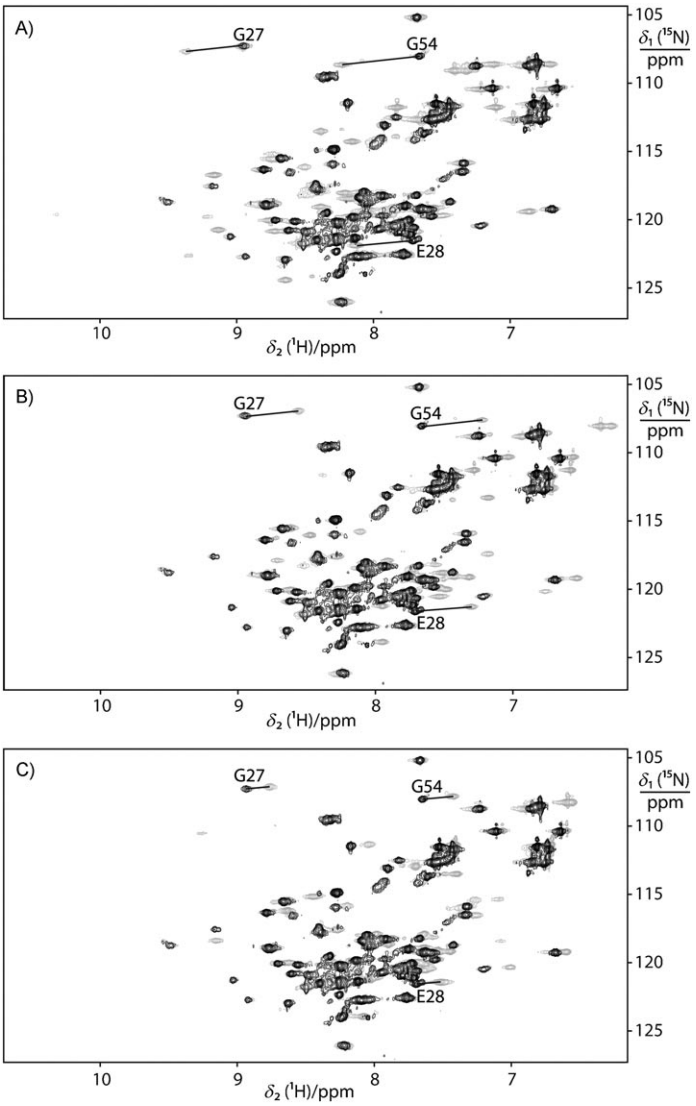

Figure 1. ^{15}N HSQC spectra of ArgN–4MDPA in complex with different metal ions. The spectra were recorded by using 0.15 mM solutions of ^{15}N-labelled ArgN–4MDPA in 20 mM 2-(*N*-morpholino)ethanesulfonic acid (MES) buffer, pH 6.5, on a Bruker 600 MHz NMR spectrometer at 25 °C. Selected pairs of cross-peaks from the diamagnetic and paramagnetic molecules are connected by lines and labelled with their assignment. A) Superimposition of ^{15}N HSQC spectra recorded with Y^{3+} (black) and Tb^{3+}/Y^{3+} in a ratio of 1:0.8 (grey). B) As in A), except that the grey spectrum was recorded with Tm^{3+}/Y^{3+}. C) As in A), except that the grey spectrum was recorded with Yb^{3+}/Y^{3+}.

was virtually identical to that of the ArgN–4MDPA–Yb^{3+} complex, indicating that the binding affinity of ArgN–4DPA was greater than that of DPA (data not shown).

Larger PCSs were observed for the corresponding complexes of p75ICD–4MDPA. For example, Tm^{3+} produced PCSs greater than 5 ppm (Figure 2). The complex with Co^{2+}, however, showed significant PCSs but also severe line broadening, which may have been caused by binding of Co^{2+} to the N-terminal His_6 tag (data not shown). Because paramagnetic relaxation enhancements (PREs) from highly paramagnetic lanthanides cause cross-peaks from amides close to the metal ion to disappear, we also measured complexes of p75ICD–4MDPA with the weakly paramagnetic lanthanides Ce^{3+}, Eu^{3+} and Nd^{3+} for improved accuracy of the metal position in the $\Delta\chi$-tensor fits.

The assignment of the cross-peaks in the paramagnetic state used the fact that paramagnetic peaks are displaced along approximately parallel lines from the corresponding diamagnetic peaks and that cross-peaks observed with different metal ions mostly align along the same line.[10,26] After determination of initial $\Delta\chi$ tensors, PCSs of unassigned peaks were predicted by the program Numbat[27] allowing additional assignments that were used to refine the $\Delta\chi$ tensor in several rounds of assignment and $\Delta\chi$-tensor refinement.

Metal position and $\Delta\chi$ tensors: The final $\Delta\chi$ tensors were determined in a fit by using a common metal position for all paramagnetic metal ions, that is, Ce^{3+}, Tb^{3+}, Tm^{3+}, Yb^{3+} and Co^{2+} for ArgN–4MDPA (Table S2 in the Supporting Information) and Ce^{3+}, Nd^{3+}, Eu^{3+}, Tb^{3+}, Tm^{3+} and Yb^{3+} for p75ICD–4MDPA (Table S4). The PCSs of most amides of the ArgN–4MDPA–Ln^{3+} complexes were smaller and of opposite sign compared with those of the corresponding complexes of ArgN–4MMDPA.[18] The smaller magnitudes of the $\Delta\chi$ tensors suggest increased mobility of the 4MDPA tag, resulting in partial averaging of the PCSs. This view is supported by the $\Delta\chi$-tensor fits, which positioned the metal ion too far from any carboxyl group of the protein for any contacts (Figure 3 A). This indicates that the position of the metal ion is primarily restrained by the restricted conformational space accessible to the tag.

The p75ICD–4MDPA–Ln^{3+} complexes produced large PCSs despite high solvent exposure of Cys416. In a previous study of p75ICD with a 4MMDPA tag attached to Cys416, lanthanide ions were found to bind not only to the DPA moiety but also to the carboxyl group of Asp397,[25] which is located on a different helix.[24] In the case of the p75ICD–4MDPA construct, however, fitting of the PCSs (Table S3 in the Supporting Information) to the NMR structure (PDB code 1NGR)[24] indicated that the distance between the metal ion and the carboxyl group of Asp397 was too long for direct contacts due to the absence of the methylene

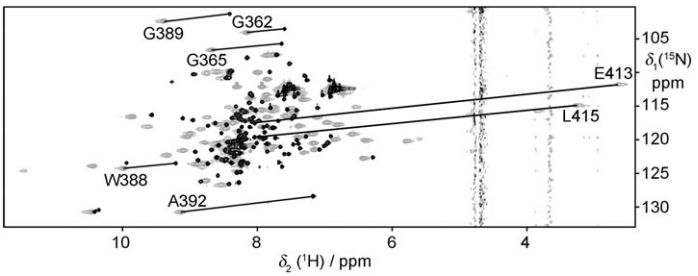

Figure 2. Superimposition of ^{15}N HSQC spectra of p75ICD–4MDPA in complex with Y^{3+} (black) and Tm^{3+} (grey). The spectra were recorded by using 0.15 mM solutions of ^{15}N-labelled p75ICD–4MDPA in 20 mM HEPES buffer (pH 7.0) and 100 mM NaCl at 25 °C on a Bruker 800 MHz NMR spectrometer.

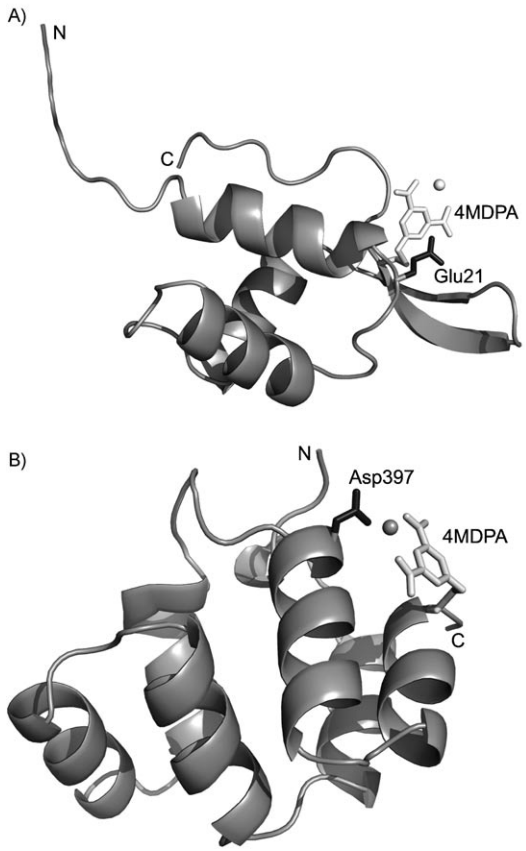

Figure 3. Ribbon representations of the ArgN–4MDPA and p75ICD–4MDPA constructs. The conformation of 4MDPA has been modelled, with the metal position determined by the $\Delta\chi$-tensor fit highlighted by a sphere. A) The first conformer of the NMR structure of ArgN (PDB code 1AOY),[23] showing the side chains of Cys68 and 4MPDA (light grey) and Glu21 (black) in a heavy-atom representation. B) Structure of the death domain of p75ICD calculated by using PCS–Rosetta.[41] The side chains of Cys416 and 4MPDA (light grey) and Asp397 (black) are shown in a heavy-atom representation.

group in 4MDPA. This was unexpected, as the lanthanide ions in the p75ICD–4MDPA–Ln^{3+} complexes produced $\Delta\chi$ tensors at least as large as any reported to date for DPA complexes,[18,20,25,28] suggesting that the metals were well immobilised. A structural change caused by the metal appears unlikely, as chemical shifts were very similar in the presence and absence of diamagnetic Y^{3+}. Considering that the NMR structure had been calculated with a limited number of NOEs and without long-range restraints such as PCSs, we used PCS–Rosetta[41] to calculate a model that fulfils the PCSs better than the original NMR structure.

The PCS–Rosetta calculations used the established Rosetta protocol for fragment selection,[29] except that the data base of protein structures was spiked with 110 known 3D structures of death domains. All available experimental PCSs (Table S3 in the Supporting Information) were used simultaneously to improve the yield of correctly folded structures in the fragment assembly step and to identify the structure with the lowest combined Rosetta and PCS energy. The structure with the best score showed the same fold as the NMR structure with a backbone root mean square deviation (rmsd) of 1.7 Å and fulfilled the PCSs with much smaller residual violations. Repeating the fitting procedure described for ArgN–4MDPA positioned the metal ion within the usual Ln^{3+}–oxygen contact distance[30] of Asp397 (Figure 3B), suggesting that this contact is important for immobilising the lanthanides. Notably, the distance between the C_β atoms of Cys416 and Asp397 differs by no more than 0.5 Å between the PCS–Rosetta structure and the original NOE structure. The largest difference between the two structures is the position of the first helix of the death-domain fold (Figure S5 in the Supporting Information) where the PCSs fitted least well in the NOE structure. Therefore, the improved position of the lanthanide in the PCS–Rosetta structure originated from improved $\Delta\chi$-tensor fits rather than a structural difference in the metal binding site.

Discussion

Synthesis of the 4MDPA dimer: The synthesis of the 4MDPA dimer is readily achieved from chelidamic acid. Compared to 4MMDPA,[18] the synthetic protocol of Scheme 2 has the same number of steps but all steps are easier and faster to perform, resulting in a high overall yield. In contrast to 4MMDPA, the protocol results in a reagent that spontaneously reacts with cysteine thiol groups.

Ligation protocol and yield: Many of the published tags designed to form disulfide bonds with cysteine residues are activated either as methanethiosulfonates (MTS)[31] or by a pyridylthio group.[32] This makes them convenient to use as they will spontaneously react with a cysteine thiol group. Alternatively, instead of chemically activating the tag, the protein thiol groups can be activated by using Ellman′s reagent (5,5′-dithiobis-(2-nitrobenzoic acid, DTNB) to form a mixed disulfide with thionitrobenzoate (TNB). TNB is a good leaving group that is easily replaced by a thiol-containing tag, converting the protein into a new mixed disulfide with the tag molecule.[14,17,18,20]

The 4MDPA dimer is a reagent analogous to the Ellman reagent, that is, one half of the reagent reacts with the cysteine thiol group, whereas the other half acts as a leaving group. To prevent protein dimerisation through disulfide bond formation, the reaction of native protein with tagged protein molecules must be avoided. Therefore we recommend adding the target protein to the solution containing excess 4MDPA dimer rather than the other way around. The same reasoning applies to other water-soluble tags activated as MTS or by a pyridylthio group. The only fundamental difference between these conventional tags and the 4MDPA dimer is that one of the two 4MDPA moieties of the dimer acts as the leaving group and, therefore, cannot ligate with the protein. The use of the 4MDPA dimer in 4–5 molar excess produced very high reaction yields, making subsequent chromatographic separation of tagged and un-

tagged protein unnecessary. In addition, excess reagent is easily removed by ultrafiltration and can be recycled for another reaction.

Metal immobilisation: Because PCSs can be positive or negative, mobility of the tag tends to reduce PCSs significantly.[12,18,33,34] In addition, PCSs that are averaged due to movement of the metal ion with respect to the protein cannot be accurately fitted by a single $\Delta\chi$ tensor. Immobilisation of the metal ion on the protein surface is thus important.

It has been shown that lanthanides are best immobilised by tags that are linked to the protein through two attachment points[7,13,15,16,19] and that DPA tags can mimic the two-point attachment situation, as they leave free coordination sites on the lanthanide to bind to carboxyl groups of the protein.[18,20] In the case of the 4MMDPA tag, we find that large PCSs are obtained when a carboxyl group is positioned about 5–6 Å from the cysteine thiol group to which the tag is attached.[10,18] For the 4MDPA tag, a correspondingly shorter distance is expected to be optimal, although the greater magnitude of electrostatic forces near the protein surface[35] may assist immobilisation of the metal also without direct contacts with protein carboxyl groups. In the case of the ArgN–4MDPA adduct, the lanthanide ion seems to be immobilised already by steric constraints without coordination by a protein carboxyl group. Clearly, the exceptional rigidity of the 4MDPA tag, which has only a single rotatable bond beyond the disulfide bridge through which it is attached to the protein, facilitates the relay of steric restraints of the disulfide bond to the lanthanide.

$\Delta\chi$-Tensor magnitudes and orientations: Large $\Delta\chi$ tensors are a prerequisite for large PCSs and large residual dipolar couplings (RDCs) arising from the concomitant molecular alignment in the external magnetic field. In the case of the ArgN–4MDPA adduct, the $\Delta\chi$ tensors of most metal ions were similar in magnitude to those previously measured for ArgN–3MDPA,[20] that is, about half as large as those observed for ArgN–4MMDPA. In contrast, the $\Delta\chi$ tensors of the p75ICD–4MDPA construct are as large or larger than those observed for any DPA-tagged protein in our laboratory, including the p75ICD–4MMDPA complex.[25] Interestingly, PCSs induced by 4MDPA and 4MMDPA tags were very different in the case of ArgN, but similar (though not the same) in the case of p75ICD (Figures S6 and S7 in the Supporting Information). This suggests that, in the case of the 4MDPA and 4MMDPA constructs of p75ICD, the lanthanide is similarly coordinated by the DPA tag and a protein carboxyl group. In contrast, 4MDPA and 4MMDPA lead to different coordination of the metal ions in the case of ArgN, which may be explained by the difficulty to assist the metal coordination by a protein carboxyl group in the 4MDPA construct. Importantly, the results obtained with both proteins show that small differences between different DPA tags lead to significantly different PCSs and thus, $\Delta\chi$ tensors, offering a convenient way of obtaining complementary data without further engineering of the protein.

Conclusion

4MDPA presents a new lanthanide binding tag, which is as small as the previously described 3MDPA tag but more symmetrical. With only a single rotatable bond between the DPA moiety and the disulfide bond formed with a cysteine residue of the target protein, the tag can immobilise lanthanide ions more easily than tags with longer tethers. In addition, electrostatic interactions with carboxyl groups of the protein can further stabilise the position of the lanthanide. Finally, the reactivity of the 4MDPA dimer makes the tagging reaction exceedingly easy to perform. Thus, the 4MDPA dimer presents a very attractive reagent for tagging proteins site-specifically with lanthanide ions, enabling a wealth of paramagnetic studies.[36]

Experimental Section

General: Chelidamic acid monohydrate (**1**) was purchased from Sigma–Aldrich or synthesised from sodium alcohol and acetone following a published protocol.[37] ^{1}H and $^{13}C\{^{1}H\}$ NMR spectra were recorded on a Varian Mercury 400 MHz NMR spectrometer operating at a ^{1}H NMR frequency of 400 MHz. All NMR spectra were acquired at 25 °C and chemical shifts were internally referenced to residual solvent peaks.

Di-*tert*-butyl-chelidamate: Chelidamic acid monohydrate (**1**) (1.00 g, 4.97 mmol) was suspended in CH_2Cl_2 (20 mL) and an aqueous $HClO_4$ solution (70%, 645 μL, 7.5 mmol) was added. The suspension was cooled to −40 °C and liquid isobutylene (10 mL) was then added. The reaction flask was tightly sealed and the reaction mixture was allowed to warm to room temperature. The suspension was stirred at room temperature for 12 h. The resulting homogenous solution was cooled to −20 °C and slowly poured into saturated aqueous sodium bicarbonate solution. The mixture was extracted with ethyl acetate (3×50 mL) and the combined organic phases were washed with brine (100 mL), dried over anhydrous sodium sulfate, filtered and evaporated under reduced pressure to yield a pale yellow solid (1.11 g, 75%). The crude product was used without further purification. ^{1}H NMR (400 MHz, $CDCl_3$): $\delta = 7.11$ (s, 2H), 1.54 ppm (s, 18H); ^{13}C NMR (100 MHz, $CDCl_3$): $\delta = 181.20$, 160.30, 137.47, 120.09, 85.19, 27.84 ppm.

Di-*tert*-butyl-4-thioxo-1-hydropyridine-2,6-dicarboxylate (2): Di-*tert*-butyl-chelidamate (250 mg, 0.847 mmol) and Lawesson's reagent (174 mg, 0.430 mmol) were dissolved in dry toluene (5 mL). The reaction mixture was stirred under nitrogen atmosphere at room temperature for approximately two hours. When there was no starting material left (TLC control, mobile phase: hexane/EtOAc 1:1) the reaction mixture was applied directly to a pre-eluted (hexane/EtOAc 5:1) silica gel column. The column was eluted with hexane/EtOAc (5:1) and when bright yellow fractions started to emerge, the mobile phase was changed to toluene. Bright orange fractions containing high concentrations of the product were evaporated under reduced pressure to afford a bright orange solid, which was crystallised from hexane/EtOAc to give compound **2** (160 mg, 74%). ^{1}H NMR (400 MHz, $CDCl_3$): $\delta = 7.98$ (s, 2H), 1.60 ppm (s, 18H); ^{13}C NMR (100 MHz, $CDCl_3$): $\delta = 160.50$, 132.13, 85.62, 27.86 ppm.

Tetra-*tert*-butyl-4,4′-disulfanediyldipyridine-2,6-dicarboxylate (3): Tetrabutylammonium chloride (220 mg) and an aqueous solution of hydrogen peroxide (10%, 12 mL) were added to the solution of di-*tert*-butyl-4-thioxo-1,4-dihydropyridine-2,6-dicarboxylate (**2**) (500 mg, 1.61 mmol) in CH_2Cl_2 (100 mL). The suspension was stirred intensively at room temperature for approximately 2 h. When there was no starting material left (TLC control, mobile phase: hexane/EtOAc 2:1) the phases were separated and the organic phase was washed with water (100 mL) and brine (100 mL), dried over anhydrous sodium sulfate, filtered and the solvent was removed under reduced pressure. The residue was purified on a

silica gel column (mobile phase: hexane/EtOAc with gradient from 5:1 to 2:1) to yield compound **3** (372 mg, 75%) as a white foam. ^{1}H NMR (400 MHz, $CDCl_3$): $\delta = 8.23$ (s, 4H), 1.61 ppm (s, 36H); ^{13}C NMR (100 MHz, $CDCl_3$): $\delta = 162.61$, 150.09, 148.93, 123.26, 83.16, 27.92 ppm; MS (ES$^+$): m/z calcd for $C_{30}H_{41}N_2O_8S_2$: 621.2 $[M+H]^+$; found: 621.6; HRMS (TOF ES$^+$): m/z calcd for $C_{30}H_{40}N_2O_8NaS_2$: 643.2124 $[M+Na]^+$; found: 643.2117.

4,4′-Disulfanediyldipyridine-2,6-dicarboxylic acid (4): Trifluoroacetic acid (1.5 mL) was added to a solution of disulfide **3** (130 mg, 0.209 mmol) in dry CH_2Cl_2 (3 mL). The reaction mixture was stirred at room temperature for 8 h and during this period a precipitate formed. It was filtered, washed with CH_2Cl_2 (3×3 mL) and dried under reduced pressure to yield product **4** as a white powder (68 mg, 82%). ^{1}H NMR (400 MHz, [D$_6$]DMSO): $\delta = 8.31$ ppm (s, 4H); ^{13}C NMR (100 MHz, [D$_6$]DMSO): $\delta =$ 165.33, 149.53, 149.42, 123.71 ppm; HRMS (ES$^-$): m/z calcd for $C_{14}H_8N_2O_8S_2$: 394.9644 $[M-H]^-$; found: 394.9644.

Ligation of proteins with 4MDPA: All steps were performed at room temperature. ArgN or p75ICD (0.5 mL, 1 mM) were first reduced with dithiothreitol (DTT; 5 equiv) at pH 7.0. The reducing agent was removed by washing with reaction buffer (50 mM sodium phosphate, pH 7.0) by using a Millipore ultrafilter with a molecular weight cutoff of 3 kDa or a PD-10 column (GE Healthcare). A solution of 4MDPA dimer **4** (20 equiv) in the reaction buffer (3 mL) was prepared and the pH was adjusted to 7.0. The protein was added drop-wise to the solution of 4MDPA dimer, the remaining solution was incubated at room temperature overnight and subsequently purified by FPLC on a SP sepharose column for ArgN–4MDPA and a DEAE sepharose column for p75ICD–4MDPA.

Metal binding and exchange: Complexes with lanthanides were formed by titrating the protein solutions (buffered at pH 6.5 or 7.0, see below) with aqueous stock solutions (10 mM) of $LnCl_3$ up to a molar ratio of 1:1. To swap between different lanthanides, the metal-free forms of the protein–4MDPA adducts were regenerated by treatment with 10-fold excess of diethylene triamine pentaacetic acid (DTPA) followed by chromatographic purification of ArgN–4MDPA and p75ICD–4MDPA on SP and DEAE sepharose columns, respectively. Following exchange into the respective NMR buffers, the samples were ready for titration with a new metal ion.

NMR measurements: NMR measurements of ArgN–4MDPA and p75ICD–4MDPA were performed at 25°C in MES (20 mM, pH 6.5) and HEPES/NaCl (20 mM/100 mM, pH 7.0) buffer, respectively, by using Bruker 600 or 800 MHz NMR spectrometers equipped with cryoprobes. PCSs were calculated as the ^{1}H chemical shift of the protein in the paramagnetic state minus the ^{1}H chemical shift of the corresponding resonances in the diamagnetic state.

PCS–Rosetta calculations: PCS–Rosetta used the Rosetta protocol supplemented with additional PCS restraints.[41] To calculate a model of p75ICD, 10000 models were assembled from fragments selected by the usual Rosetta protocol following the addition of 110 3D structures of death domain proteins to the database to bias the selection towards correct fragments. The fragment assembly step was supported by PCSs. The five models with the best combined Rosetta and PCS score were submitted to all-atom refinement without using PCS restraints generating 100 structures for each model. The final models were scored by using the combined Rosetta and PCS score. The model with the best score was used for further fitting of the $\Delta\chi$ tensors.

Fitting of $\Delta\chi$ tensors: To avoid the possibility that the paramagnetic centre is positioned too far from the protein and consequently associated with a too large $\Delta\chi$ tensor (or positioned too close with a too small $\Delta\chi$ tensor), the covalent structures of the tagged proteins were taken into account. First, the 4MDPA tag was connected by a disulfide bond to the tagged cysteine residue. The metal ion was rigidly positioned between the carboxyl groups of the tag at the position observed in the crystal structure of the $[Ln(dpa)_3]^{3-}$ complex.[38] Next, 10000 conformations were generated by randomly varying the χ_1 and χ_2 dihedral angles of the cysteine residue as well as the dihedral angle of the bond between the sulfur and the aromatic ring of 4MDPA. The dihedral angle of the disulfide bond was allowed to assume values between −100 and −80° or 80 and 100° (the angles usually displayed by disulfide bonds.[39]) Conformations leading to steric clashes with the protein were eliminated. To allow for some flexibility of amino acid side chains, hydrogen atoms were omitted and each heavy atom was represented by a sphere of 0.75 Å radius (i.e., less than van der Waals radius). This also accelerated the computations. The $\Delta\chi$ tensors were fitted by using the metal positions of the remaining (typically 1000–2000) conformations, where each fit used the same position for all metal ions. The best fit was used for plotting the structure of the protein-4MDPA-metal complex. As a measure of the precision of the metal position, the standard deviation of the metal position of the twenty best-fitting conformations from the position in the best-fitting model was determined. As a measure of the precision of the $\Delta\chi$ tensors, the fits to the best-fitting model were repeated 100 times, omitting 20% of the data from each metal ion in a Monte-Carlo protocol.[27]

Acknowledgements

Financial support by the Australian Research Council, including a Future Fellowship to T.H., is gratefully acknowledged. We thank Dr. Hiromasa Yagi for the expression vector of the p75ICD C379S mutant.

[1] M. Allegrozzi, I. Bertini, M. B. L. Janik, Y. M. Lee, G. Liu, C. Luchinat, *J. Am. Chem. Soc.* **2000**, *122*, 4154–4161.
[2] I. Bertini, C. Luchinat, G. Parigi, *Prog. Nucl. Magn. Reson. Spectrosc.* **2002**, *40*, 249–273.
[3] I. Bertini, G. A. Giachetti, C. Luchinat, G. Parigi, M. V. Petoukhov, R. Pierattelli, E. Ravera, D. I. Svergun, *J. Am. Chem. Soc.* **2010**, *132*, 13553–13558.
[4] M. A. S. Hass, P. H. J. Keizers, A. Blok, Y. Hiruma, M. Ubbink, *J. Am. Chem. Soc.* **2010**, *132*, 9952–9953.
[5] J. C. Hus, D. Marion, M. Blackledge, *J. Mol. Biol.* **2000**, *298*, 927–936.
[6] P. H. J. Keizers, B. Mersinli, W. Reinle, J. Donauer, Y. Hiruma, F. Hannemann, M. Overhand, R. Bernhardt, M. Ubbink, *Biochemistry* **2010**, *49*, 6846–6855.
[7] T. Saio, M. Yokochi, H. Kumeta, F. Inagaki, *J. Biomol. NMR* **2010**, *46*, 271–280.
[8] G. Otting, *Annu. Rev. Biophys.* **2010**, *39*, 387–405.
[9] F. Rodriguez-Castañeda, P. Haberz, A. Leonov, C. Griesinger, *Magn. Reson. Chem.* **2006**, *44*, S10–S16.
[10] X. C. Su, G. Otting, *J. Biomol. NMR* **2009**, *46*, 101–112.
[11] a) V. Gaponenko, A. S. Altieri, J. Li, R. A. Byrd, *J. Biomol. NMR* **2002**, *24*, 143–148; b) A. Dvoretsky, V. Gaponenko, P. R. Rosevear, *FEBS Lett.* **2002**, *528*, 189–192; c) A. Leonov, B. Voigt, F. Rodriguez-Castañeda, P. Sakhaii, C. Griesinger, *Chem. Eur. J.* **2005**, *11*, 3342–3348; d) P. Haberz, F. Rodriguez-Castañeda, J. Junker, S. Becker, A. Leonov, C. Griesinger, *Org. Lett.* **2006**, *8*, 1275–1278; e) D. Häussinger, J. Huang, S. Grzesiek, *J. Am. Chem. Soc.* **2009**, *131*, 14761–14767.
[12] T. Ikegami, L. Verdier, P. Sakhaii, S. Grimme, B. Pescatore, K. Saxena, F. M. Fiebig, C. Griesinger, *J. Biomol. NMR* **2004**, *29*, 339–349.
[13] M. Prudêncio, J. Rohovec, J. A. Peters, E. Tocheva, M. J. Boulanger, M. E. P. Murphy, H. J. Hupkes, W. Kosters, A. Impagliazzo, M. Ubbink, *Chem. Eur. J.* **2004**, *10*, 3252–3260.
[14] X. C. Su, T. Huber, N. E. Dixon, G. Otting, *ChemBioChem* **2006**, *7*, 1599–1604.
[15] M. D. Vlasie, C. Comuzzi, A. van den Nieuwendijk, M. Prudêncio, M. Overhand, M. Ubbink, *Chem. Eur. J.* **2007**, *13*, 1715–1723.
[16] P. H. J. Keizers, J. F. Desreux, M. Overhand, M. Ubbink, *J. Am. Chem. Soc.* **2007**, *129*, 9292–9293.
[17] X. C. Su, K. McAndrew, T. Huber, G. Otting, *J. Am. Chem. Soc.* **2008**, *130*, 1681–1687.
[18] X. C. Su, B. Man, S. Beeren, H. Liang, S. Simonsen, C. Schmitz, T. Huber, B. A. Messerle, G. Otting, *J. Am. Chem. Soc.* **2008**, *130*, 10486–10487.

[19] T. Saio, K. Ogura, M. Yokochi, Y. Kobashigawa, F. Inagaki, *J. Biomol. NMR* **2009**, *44*, 157–166.
[20] B. Man, X. C. Su, H. B. Liang, S. Simonsen, T. Huber, B. A. Messerle, G. Otting, *Chem. Eur. J.* **2010**, *16*, 3827–3832.
[21] I. Grenthe, *J. Am. Chem. Soc.* **1961**, *83*, 360–364.
[22] G. Pintacuda, A. Moshref, A. Leonchiks, A. Sharipo, G. Otting, *J. Biomol. NMR* **2004**, *29*, 351–361.
[23] M. Sunnerhagen, M. Nilges, G. Otting, J. Carey, *Nat. Struct. Biol.* **1997**, *4*, 819–826.
[24] E. Liepinsh, L. L. Ilag, G. Otting, C. F. Ibáñez, *EMBO J.* **1997**, *16*, 4999–5005.
[25] A. Potapov, H. Yagi, T. Huber, S. Jergic, N. E. Dixon, G. Otting, D. Goldfarb, *J. Am. Chem. Soc.* **2010**, *132*, 9040–9048.
[26] M. John, A. Y. Park, G. Pintacuda, N. E. Dixon, G. Otting, *J. Am. Chem. Soc.* **2005**, *127*, 17190–17191.
[27] C. Schmitz, M. J. Stanton-Cook, X. C. Su, G. Otting, T. Huber, *J. Biomol. NMR* **2008**, *41*, 179–189.
[28] X. C. Su, H. Liang, K. V. Loscha, G. Otting, *J. Am. Chem. Soc.* **2009**, *131*, 10352–10353.
[29] R. Das, D. Baker, *Annu. Rev. Biochem.* **2008**, *77*, 363–382.
[30] D. Parker, R. S. Dickins, H. Puschmann, C. Crossland, J. A. K. Howard, *Chem. Rev.* **2002**, *102*, 1977–2010.
[31] D. J. Smith, E. T. Maggio, G. L. Kenyon, *Biochemistry* **1975**, *14*, 766–771.
[32] G. N. Zecherle, A. Oleinikov, R. R. Traut, *J. Biol. Chem.* **1992**, *267*, 5889–5896.
[33] I. Bertini, C. Del Bianco, I. Gelis, N. Katsaros, C. Luchinat, G. Parigi, M. Peana, A. Provenzani, M. A. Zoroddu, *Proc. Natl. Acad. Sci. USA* **2004**, *101*, 6841–6846.
[34] I. Bertini, Y. K. Gupta, C. Luchinat, G. Parigi, M. Peana, L. Sgheri, J. Yuan, *J. Am. Chem. Soc.* **2007**, *129*, 12786–12794.
[35] V. Z. Spassov, R. Ladenstein, A. D. Karshikoff, *Protein Sci.* **1997**, *6*, 1190–1196.
[36] G. Otting, *J. Biomol. NMR* **2008**, *42*, 1–9.
[37] M. Achmatowicz, L. S. Hegedus, S. David, *J. Org. Chem.* **2003**, *68*, 7661–7666.
[38] J. M. Harrowfield, Y. Kim, B. W. Skelton, A. H. White, *Aust. J. Chem.* **1995**, *48*, 807–823.
[39] N. L. Haworth, J. E. Gready, R. A. George, M. A. Wouters, *Mol. Simul.* **2007**, *33*, 475–485.
[40] S. Simonsen, unpublished results.
[41] C. Schmitz, R. Vernon, G. Otting, D. Baker, T. Huber, unpublished results.

Received: December 10, 2010
Published online: May 3, 2011

